

# RSC Advances



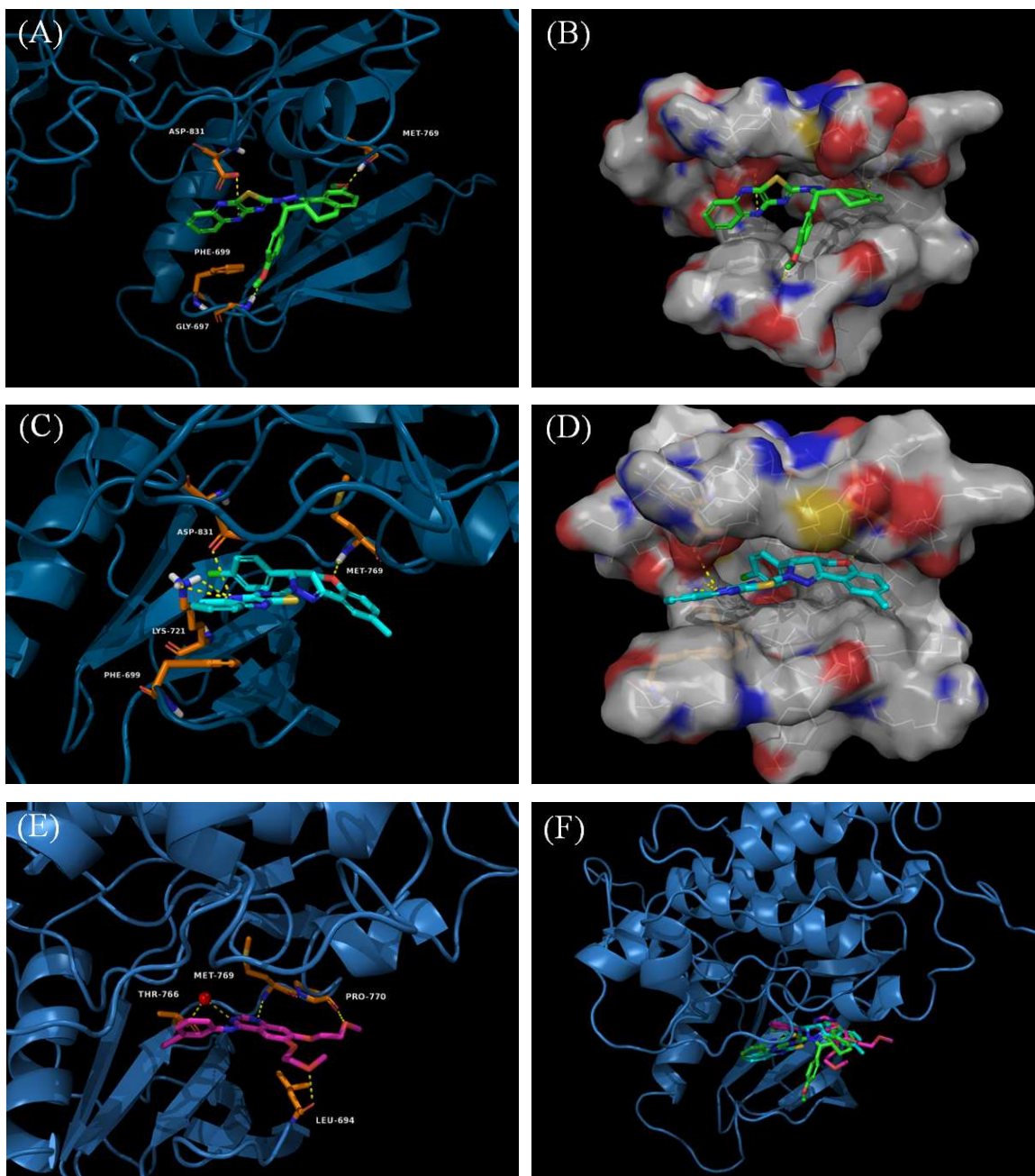
This is an *Accepted Manuscript*, which has been through the Royal Society of Chemistry peer review process and has been accepted for publication.

*Accepted Manuscripts* are published online shortly after acceptance, before technical editing, formatting and proof reading. Using this free service, authors can make their results available to the community, in citable form, before we publish the edited article. This *Accepted Manuscript* will be replaced by the edited, formatted and paginated article as soon as this is available.

You can find more information about *Accepted Manuscripts* in the [Information for Authors](#).

Please note that technical editing may introduce minor changes to the text and/or graphics, which may alter content. The journal's standard [Terms & Conditions](#) and the [Ethical guidelines](#) still apply. In no event shall the Royal Society of Chemistry be held responsible for any errors or omissions in this *Accepted Manuscript* or any consequences arising from the use of any information it contains.

## Graphical Abstract



A series of pyrazole-quinoxaline derivatives have been synthesized and most of them exhibited potent affinity for EGFR or HER-2 kinase as well as excellent antiproliferative activities. Compounds **41** was the most active.

**Discovery of 3,3a,4,5-tetrahydro-2H-benzo[g]indazole containing quinoxaline derivatives as novel EGFR/HER-2 dual inhibitors**

**Xi Zong<sup>a</sup>, Jin Cai<sup>a</sup>, Junqing Chen<sup>a</sup>, Chunlong Sun<sup>a</sup>, Lushen Li<sup>b</sup>, Min Ji<sup>b,c,\*</sup>**

*<sup>a</sup> School of Chemistry & Chemical Engineering, Southeast University, Nanjing 210096, China*

*<sup>b</sup> School of Biological Science & Medical Engineering, Southeast University, Nanjing 210096, China*

*<sup>c</sup> Suzhou Key Laboratory of Biomaterials and Technologies & Collaborative Innovation Center of Suzhou Nano Science and Technology, Suzhou, 215123, China*

\*Corresponding author. Tel. & fax: +86-0512-62729923; e-mail: [jimin@seu.edu.cn](mailto:jimin@seu.edu.cn).

**Abstract**

In the present study, twenty five pyrazole-quinoxaline derivatives (**4a–4y**) have been designed and synthesized; their biological activities were evaluated as potential EGFR, HER-2 kinase inhibitors. Among them, compound **4l** manifested better antiproliferative activity against A549 and MCF-7 cell lines as compared to **Eroltinib**. Further kinase inhibitory activity assay results indicated that compound **4l** demonstrates the most potent enzyme inhibitory activity. Docking simulation was further performed to position compounds **4l** and **4x** into the active binding site of EGFR to determine the probable binding model. The 3D-QSAR models were built for reasonable design of EGFR inhibitors at present and in future. These discoveries suggested that title compounds are potential EGFR/HER-2 dual inhibitors and compound **4l** may be promising lead compound for the development of novel antitumor agent potentially via inhibiting EGFR/HER-2.

**Keywords:**

Anticancer

Pyrazole-quinoxaline derivatives

EGFR/HER-2

Molecular docking

3D - QSAR

## 1. Introduction

Cancer, as a major problem of human health in the world, is continuing the second cause of mortality worldwide with over millions of cases every year<sup>1</sup>. Molecularly targeted therapeutics, which is highly selective and not associated with the serious toxicities induced by conventional cytotoxic drugs, has become an attractive approach for cancer chemotherapy<sup>2</sup>. Protein kinases catalyze the phosphorylation of tyrosine and serine/threonine residues in various proteins<sup>3</sup>, thus, protein kinases are extensively targeted for the discovery of inhibitors as potential cancer-treatment drugs<sup>4-7</sup>. In recent years, a variety of novel anticancer lead compounds target mutant or aberrantly expressed oncogenic growth factor receptor and nonreceptor tyrosine kinases in mitogenic or proliferative signal transduction pathways of cancer cells<sup>8</sup>.

As a transmembrane protein tyrosine kinase (PTK), the epidermal growth factor receptor (EGFR) family plays a crucial role in regulating cell proliferation, survival, adhesion, migration, differentiation and apoptosis and has been identified as a critical role in cancer<sup>9, 10</sup>. The EGFR family consists of human epidermal growth factor receptor (EGFR/ErbB-1), human epidermal growth factor receptor 2 (HER-2/ErbB-2), human epidermal growth factor receptor 3 (HER-3/Erb-3), and human epidermal growth factor receptor 4 (HER-4/Erb-4)<sup>11</sup>. Among them, as the targets in current cancer research, EGFR and HER-2 have been implicated in the development and malignancy of many human cancers<sup>7</sup>, because their over expression or abnormal activation often cause cell malignant transformation, such as non-small-cell lung cancer (NSCLC), prostate, breast, stomach, colon, and ovarian cancers<sup>12-15</sup>.

Recently, thousands of small organic molecules with different structures have been developed as multi-target inhibitors<sup>16-18</sup>. Compounds that inhibit the kinase activity of EGFR and/or HER-2 after binding to its ATP binding site are of potential interest as new therapeutic antitumor agents<sup>19</sup>. A number of tyrosine kinase inhibitors (TKIs) targeting EGFR and HER-2 have been approved for clinical treatment of cancer by FDA. As shown in **Fig. 1**, the EGFR inhibitors **Gefitinib**, **Erlotinib**, **Lapatinib**, **Vandetanib**, **Icotinib** and **Afatinib** have been marketed and launched successfully to treat various kinds of cancer in clinical. There are also several EGFR kinase inhibitors, such as **Dacomitinib** are already showing promise in phase III clinical trials.

In previous study, several pyrazole derivatives have been reported to possess a wide range of bioactivities. The pyrazole moiety makes up the core structure of numerous biologically active compounds, such as antiviral/antitumor<sup>20-22</sup>, antibacterial<sup>23, 24</sup>,

antiinflammatory<sup>25</sup>, analgesic<sup>26</sup>, fungistatic<sup>27</sup>, and antihyperglycemic<sup>28</sup> agents. Recently, special attention has been imposed on the usage of pyrazole for anticancer. Lv *et al.* reported a series of novel pyrazole derivatives (**PD**, **Fig. 1**) which showed modest to potent EGFR TK inhibitory activity<sup>29</sup>. In addition, a series of novel EGFR and HER-2 inhibitors (**N1**, **N2**, **Fig. 1**) have been discovered with thiazolyl-pyrazoline scaffold<sup>30, 31</sup>. Moreover, it was demonstrated that quinoxaline derivatives display a broad spectrum of biological activities; some of these compounds have been described as potential candidates for the treatment of cancer<sup>32-34</sup>.

However, to our knowledge, few reports have been dedicated to design and synthesize a type of antitumor compound that contains pyrazole and quinoxaline simultaneously. A perusal of the literature revealed that the B ring of pyrazole derivatives (**PD**, **N1** and **N2**) acts a great influence on its activity. In continuation to seek a novel scaffold as potential EGFR and HER-2 inhibitory agents, we constrain the spatial location of B ring by replacing the 3,5-diphenyl-4,5-dihydro-1H-pyrazole moiety with 3-phenyl-3,3a,4,5-tetrahydro-2H-benzo[g]indazole moiety, then integrating the novel tricyclic pyrazole derivative with thiazolo quinoxaline ring. The two combined substructures were expected to exhibit synergistic anticancer effect (**Fig. 2**).

## 2. Results and discussion

### 2.1. Chemistry

The protocol for the synthesis of novel tricyclic heterocycles containing thiazolo[4,5-b]quinoxaline derivatives (**4a-4y**) are summarized in **Scheme 1**. To explore the influence of substituted group at 4-position of phenyl and 8-position of tricyclic heterocycles on activity, compounds **4a-4o** were synthesized. We also designed compounds **4p-4y** to expand the structural diversity of the target compounds. Firstly, the diverse substituted chalcones (**2a-2y**) were afforded by treating tetralone derivatives with the appropriate aldehyde in the presence of the solution of sodium hydroxide in methanol. Secondly, cyclization of different chalcones with thiosemicarbazide in the presence of excess sodium hydroxide gave tricyclic heterocycles containing thiourea group (**3a-3y**). Finally, target compounds **4a-4y** were obtained by reacting **3a-3y** with 2, 3-dichloroquinoxaline in ethanol. All of the target compounds gave satisfactory analytical and spectroscopic data.

### 2.2. Biological activity

### 2.2.1. Antiproliferation assay

Newly synthesized derivatives **4a-4y** were assessed for their antiproliferative activities employing the MTT-based assay using **Erlotinib**, **Gefitinib** as positive control against four cultured cancer cell lines including A549, MCF-7, HeLa and HepG2 (**Table 1**). Most target compounds were found to possess broad antiproliferative activities with  $IC_{50}$  values ranging from 2.02 to 31.54  $\mu$ M. Among them, compounds **4k** and **4v** displayed the most broad-spectrum antiproliferative activities, their corresponding  $IC_{50}$  values were all below 7.00  $\mu$ M against four cancer cell lines. It is noticeable that several compounds exerted antiproliferative activities against A549 and MCF-7 cell lines comparable to the positive group drugs, such as **4b**, **4k**, **4l**, **4o**, **4q**, **4t**, **4v** and **4y**. In particular, the most significant inhibition was achieved for compound **4l** with  $IC_{50} = 1.91 \mu$ M toward MCF-7 cell line, which was better than that of **Erlotinib** ( $IC_{50} = 2.32 \mu$ M) and **Gefitinib** ( $IC_{50} = 6.26 \mu$ M). In addition, compound **4l** ( $IC_{50} = 3.04 \mu$ M) also showed higher or comparable antiproliferation against A549 cell line as compared to **Erlotinib** ( $IC_{50} = 4.28 \mu$ M) and **Gefitinib** ( $IC_{50} = 2.96 \mu$ M).

### 2.2.2 EGFR and HER-2 inhibitory activity

The principle of structural design is to verify the EGFR/HER-2 inhibitory activities of novel tricyclic heterocycles containing thiazolo[4,5-b]quinoxaline derivatives. Therefore, all compounds were assayed for their inhibitory activities against EGFR and HER-2 tyrosine kinases using **Erlotinib** as a positive control.

As showing in **Table 2**, pyrazole-quinoxaline derivatives (**4a-4y**) have demonstrated fairly good EGFR and HER-2 inhibitory activities. Subsequently structure activity relationship (SAR) analysis indicated that the substituted group at ring A ( $R_2$ ) played important roles in kinase activity, compounds substituted with electron-donating group at 4-position of ring A exhibited better potency than those with electron-withdrawing group. For example **4b** ( $IC_{50} = 2.26 \mu$ M) > **4e** ( $IC_{50} = 8.26 \mu$ M) > **4a** ( $IC_{50} = 9.82 \mu$ M) > **4d** ( $IC_{50} = 15.67 \mu$ M) > **4c** ( $IC_{50} = 21.24 \mu$ M), which was illustrated by the potency order:  $OCH_3 > CH_3 > H > Cl > F$ . In addition, compounds (**4d**, **4e**) with methyl or chlorine on the 4-position of ring A manifested more potent activities than compounds (**4g-4j**) with methyl or chlorine on the 2-position and 3-position of ring A. Compounds (**4k-4o**) with an electron-donating methoxy group on the 4-position of ring B ( $R_1$ ) displayed higher inhibitory activity than those (**4p-4y**) with methyl or hydrogen substituent. Therefore, the biological data

demonstrated that an electron-donating group substituted at the R<sub>1</sub> and/or R<sub>2</sub> position might increase the inhibitory activity against EGFR/HER-2. Replacing the 3,3a,4,5-tetrahydro-2H-benz[g]indazole ring with a 2,3,3a,4-tetrahydro[1]benzopyrano[4,3-c]pyrazole ring only resulted in a slight decrease in activity (**4a-4e** vs **4p-4t**). For the given compounds, it was observed that the IC<sub>50</sub> values of inhibitors against EGFR were consistent with that of HER-2. It was possibly attributed to high sequence homology in the catalytic domains of these two kinases and there is also a reasonable correlation between the EGFR and HER-2 inhibitory activities. Among these twenty-five pyrazole-quinoxaline derivatives, **4l** seemed to be the most potent EGFR and HER-2 inhibitor with IC<sub>50</sub> = 0.28 μM and IC<sub>50</sub> = 1.26 μM, respectively, compared with the positive control **Erlotinib** (IC<sub>50</sub> = 0.08 μM and IC<sub>50</sub> = 0.23 μM).

Taken the biological data together, we could preliminarily reach the conclusion that some target compounds are potent EGFR/HER-2 inhibitors, and are helpful for the further research of EGFR inhibitors and expanding the compound types of EGFR inhibitors.

### 2.2.3. Cytotoxicity test

As shown in **Table 3**, all the target compounds (**4a-4y**) were evaluated for their toxicity against human kidney epithelial cell 293T by the MTT assay; these compounds were tested at multiple doses to study the viability of macrophage. The median cytotoxic concentration (CC<sub>50</sub>) showed that all tested compounds were almost not cytotoxic *in vitro* against 293T.

### 2.3 Molecular docking

To further investigate the interactions between these compounds and EGFR, molecular docking of 3,3a,4,5-tetrahydro-2H-benz[g]indazole derivative **4l** and 2,3,3a,4-tetrahydro[1]benzopyrano[4,3-c]pyrazole derivative **4x** into ATP binding site of EGFR kinase were performed on the binding model based on the EGFR complex structure (1M17.pdb)<sup>35</sup>.

The docking pose of **4l** in complex with EGFR is shown in **Fig. 3A** and **B**. In the binding mode, the oxygen of methoxy moiety forms hydrogen bonding interactions with Met769 and Gly697, respectively. This may explain the reason why compound **4l** with methoxy group substituted in R<sub>1</sub> and R<sub>2</sub> could exert increased inhibitory activity against EGFR kinase. In addition, a hydrogen bonding interaction is observed between the nitrogen of the quinoxaline moiety and Asp831. Simultaneously, the terminal phenyl moiety of compound **4l** forms a π-π interaction with Phe699. As

shown in **Fig. 3C and D**, the similar  $\pi$ - $\pi$  interaction also occurs between the terminal phenyl moiety of compound **4x** and Phe699. Furthermore, the oxygen of tricyclic moiety forms hydrogen bond with Met769 and the nitrogen of the quinoxaline moiety forms hydrogen bonds with Lys721 and Asp831, respectively. Comparing these models (**Fig. 3E and F**), it is obvious that compounds **4l** and **4x** are able to nicely occupies in the active binding pocket of EGFR as well as **Erlotinib**. Interestingly, the similar hydrogen bonding interactions with Met769 were all occurred in the binding pocket of **4l**, **4x** and **Erlotinib** in complex with EGFR.

In summary, the docking analysis strongly suggests that the substituents on the two different rings and the quinoxaline moiety forms the hydrogen bonding interaction and  $\pi$ - $\pi$  interaction with the protein residues in the ATP binding site, thus causing a dramatic EGFR inhibition activities.

#### 2.4 3D-QSAR model.

To get deeper study of the quantitative structure-activity relationship on pyrazole-quinoxaline derivatives with bioactivity, a 3D-QSAR model was built according to the compounds synthesized and their corresponding capability<sup>36</sup>. Relying on the effort, we intended to explain the mechanism of the SAR, and cast a light on the discovery of more potent novel antagonist against EGFR. This model was executed by built-in QSAR software of DS 3.5(Discovery Studio 3.5, Accelrys, Co. Ltd), with all the molecular converted to the active conformation and corresponding IC<sub>50</sub> ( $\mu$ M) values transformed from an Indian medicinal chemistry lab (<http://www.sanjeevslab.org/tools-IC50.html>). By a random select, these compounds were divided into a test set containing 5 compounds and a training set comprising the rest containing 20 compounds

By default, the alignment conformation of each molecule possessed the lowest CDOCKER\_INTERACTION\_ENERGY among all of the docked poses. The critical regions (steric or electrostatic) affecting the binding affinity was gained by this 3D-QSAR model. Exerting CHARMM force field and PLS regression, the model was set up with conventional R<sup>2</sup> of 0.95, indicating this model possesses good predicting capability. The relationship between observed and predicted values has been shown graphically in **Fig. 4**.

Also the molecules aligned with the iso-surfaces of the 3D-QSAR model coefficients on electrostatic potential grids (**Fig. 5a**) and Van der Waals grids (**Fig. 5b**) were listed. Electrostatic map displayed the favorable (in blue) or unfavorable (in red)

electrostatic field region in a contour plot, while the energy grids corresponding to the favorable (in green) or unfavorable (in yellow) steric effects were also marked out. For compounds based on the 3D-QSAR model, possessing strong Van der Waals attraction in the green areas and a polar group in the blue electrostatic potential areas means achieving potent bioactivity. This model was accordant with the actual situation for potent compounds. Thus, this promising model would provide a guideline to design and optimize more effective tubulin inhibitors and pave the way for further study.

### 3. Conclusions

In this work, a series of pyrazole-quinoxaline derivatives potentially function as inhibitors of EGFR and HER-2 kinases have been synthesized, and most of them exhibited potent affinity for EGFR or HER-2 kinase as well as excellent antiproliferative activities. Compound **4I** showed excellent EGFR/HER-2 inhibition activities and better antiproliferative activities against A549 and MCF-7 cell lines as compared to **Erlotinib**. After analysis of the binding model of compounds **4I** and **4x** with EGFR, it was found that the model between compounds **4I**, **4x** and the ATP binding site were similar to that with **Erlotinib**. The quinoxaline moiety might play a crucial role in its EGFR inhibition activities by forming the  $\pi$ - $\pi$  interaction and hydrogen bonding interaction with the residues in the binding pocket. Finally, QSAR models were built with activity data and binding conformations to begin our work in this paper as well as to provide a reliable tool for reasonable design and synthesis of potent tyrosine kinase inhibitors. In conclusion, the preliminary evaluation results demonstrated that the newly tricyclic heterocycle contains pyrazole combined with thiazolo quinoxaline ring, acting as potent dual EGFR and HER-2 inhibitor, may possess therapeutic potential for cancer treatment.

## 4. Experiments

### 4.1 Materials and measurements

All chemicals and reagents used in this study were analytical grade. Thinlayer chromatography (TLC) was performed on silica gel plates with fluorescent indicator. All analytical samples were homogeneous on TLC in at least two different solvent systems. All the  $^1\text{H}$  NMR spectra were recorded on a Bruker DPX 300 model Spectrometer in  $\text{DMSO-}d_6$  and chemical shifts ( $\delta$ ) were reported as parts per million

(ppm). ESI-MS spectra were recorded on a Mariner System 5304 Mass spectrometer. Elementary analyses were performed on Elementar Vario EL III instrument.

## 4.2. Synthesis

### 4.2.1. General synthetic procedure of chalcones (**2a-2y**)

To a solution of tetralone derivatives **1a-1d** (50 mmol) and appropriate aldehyde (50 mmol) in ethanol (20 mL) was slowly added an aqueous solution of NaOH (0.012 mol, 8 N) at room temperature. The mixture was stirred for 2 h. The solid precipitate was collected by filtration and then washed by cold ethanol (30 mL) for three times. The solid was dried in vacuo to give each chalcone (**2a-2y**).

### 4.2.2. General synthetic procedure of pyrazole derivatives (**3a-3y**)

A mixture of chalcones **2a-2y** (10 mmol), thiosemicarbazide (10 mmol) and NaOH (25 mmol) in ethanol (25 ml) was refluxed for 8 h. The solution was poured into ice water and then filtered. The residue was washed with a small amount of methanol and dried in vacuo to give each pyrazole derivative respectively (**3a-3y**).

### 4.2.3. General synthetic procedure of dihydropyridin containing thiazolinone derivatives (**4a-4y**)

A mixture of pyrazole derivatives **3a-3y** (10 mmol) and 2,3-dichloroquinoxaline (10 mmol) in absolute ethanol (15 ml) was refluxed for 8 h. Progress of the reaction was monitored by TLC. After completion of the reaction, solvent was removed under reduced pressure and the residue was recrystallized from methanol to give **4a-4y**.

#### 4.2.3.1. 2-(3-Phenyl-3,3a,4,5-tetrahydro-2H-benzo[g]indazol-2-yl)thiazolo[4,5-b]quinoxaline (**4a**)

White solid. Yield 51%; m.p. 201~203°C; <sup>1</sup>H NMR (DMSO-*d*<sub>6</sub>, 300 MHz); δ: 7.94 (d, *J* = 6.4 Hz, 1H, Ar-H); 7.90 (d, *J* = 7.8 Hz, 1H, Ar-H); 7.84-7.81 (m, 2H, Ar-H); 7.63-7.53 (m, 2H, Ar-H); 7.49-7.32 (m, 2H, Ar-H); 7.30-7.28 (m, 1H, Ar-H); 7.03-6.89 (m, 4H, Ar-H); 6.08 (d, *J* = 10.7 Hz, 1H, CH); 4.10-4.03 (m, 1H, CH); 3.01-2.82 (m, 2H, CH<sub>2</sub>); 1.74-1.60 (m, 1H, CH<sub>2</sub>); 0.96-0.81 (m, 1H, CH<sub>2</sub>). ESI-MS *m/z*: 434.2 [M+H]<sup>+</sup>. Anal. Calcd for C<sub>26</sub>H<sub>19</sub>N<sub>5</sub>S (%): C, 72.03; H, 4.42; N, 16.15. Found: C, 72.43; H, 4.33; N, 16.28.

#### 4.2.3.2. 2-(3-(4-Methoxyphenyl)-3,3a,4,5-tetrahydro-2H-benzo[g]indazol-2-yl)thiazolo[4,5-b]quinoxaline (**4b**)

White solid. Yield 47%; m.p. 186~187°C; <sup>1</sup>H NMR (DMSO-*d*<sub>6</sub>, 300 MHz); δ: 8.04 (d, *J* = 7.4 Hz, 1H, Ar-H); 7.98 (d, *J* = 7.7 Hz, 1H, Ar-H); 7.86-7.84 (m, 1H, Ar-H);

7.73-7.62 (m, 2H, Ar-H); 7.48-7.36 (m, 2H, Ar-H); 7.31-7.29 (m, 1H, Ar-H); 7.12 (d,  $J = 8.2$  Hz, 2H, Ar-H); 6.91 (d,  $J = 8.5$  Hz, 2H, Ar-H); 6.10 (d,  $J = 10.6$  Hz, 1H, CH); 4.14-4.02 (m, 1H, CH); 3.70 (s, 3H, CH<sub>3</sub>); 3.02-2.86 (m, 2H, CH<sub>2</sub>); 1.84-1.81 (m, 1H, CH<sub>2</sub>); 1.06-0.96 (m, 1H, CH<sub>2</sub>). ESI-MS  $m/z$ : 464.3 [M+H]<sup>+</sup>. Anal. Calcd for C<sub>27</sub>H<sub>21</sub>N<sub>5</sub>OS (%): C, 69.96; H, 4.57; N, 15.11. Found: C, 69.85; H, 4.49; N, 15.28.

4.2.3.3. 2-(3-(4-Fluorophenyl)-3,3a,4,5-tetrahydro-2H-benzo[g]indazol-2-yl)thiazolo[4,5-b]quinoxaline (**4c**)

White solid. Yield 48%; m.p. 202~204°C; <sup>1</sup>H NMR (DMSO-*d*<sub>6</sub>, 300 MHz);  $\delta$ : 8.08 (d,  $J = 7.5$  Hz, 1H, Ar-H); 7.99-7.95 (m, 1H, Ar-H); 7.82-7.79 (m, 1H, Ar-H); 7.40-7.28 (m, 3H, Ar-H); 7.23-7.20 (m, 1H, Ar-H); 7.15-7.09 (m, 3H, Ar-H); 7.05-7.00 (m, 2H, Ar-H); 6.03 (d,  $J = 10.6$  Hz, 1H, CH); 3.87-3.37 (m, 1H, CH); 2.92-2.76 (m, 2H, CH<sub>2</sub>); 1.78-1.74 (m, 1H, CH<sub>2</sub>); 0.80-0.66 (m, 1H, CH<sub>2</sub>). ESI-MS  $m/z$ : 452.2 [M+H]<sup>+</sup>. Anal. Calcd for C<sub>26</sub>H<sub>18</sub>FN<sub>5</sub>S (%): C, 69.16; H, 4.02; N, 15.51. Found: C, 69.33; H, 4.09; N, 15.41.

4.2.3.4. 2-(3-(4-Chlorophenyl)-3,3a,4,5-tetrahydro-2H-benzo[g]indazol-2-yl)thiazolo[4,5-b]quinoxaline (**4d**)

Yellow solid. Yield 37%; m.p. 211~213°C; <sup>1</sup>H NMR (DMSO-*d*<sub>6</sub>, 300 MHz);  $\delta$ : 8.05-7.97 (m, 2H, Ar-H); 7.89-7.84 (m, 1H, Ar-H); 7.72-7.63 (m, 2H, Ar-H); 7.58-7.48 (m, 2H, Ar-H); 7.44-7.35 (m, 3H, Ar-H); 7.31-7.23 (m, 2H, Ar-H); 6.17 (d,  $J = 10.7$  Hz, 1H, CH); 4.06-4.00 (m, 1H, CH); 2.98-2.87 (m, 2H, CH<sub>2</sub>); 1.72-1.70 (m, 1H, CH<sub>2</sub>); 0.97-0.93 (m, 1H, CH<sub>2</sub>). ESI-MS  $m/z$ : 468.2 [M+H]<sup>+</sup>. Anal. Calcd for C<sub>26</sub>H<sub>18</sub>ClN<sub>5</sub>S (%): C, 66.73; H, 3.88; N, 14.97. Found: C, 66.63; H, 3.69; N, 14.78.

4.2.3.5. 2-(3-(*p*-tolyl)-3,3a,4,5-tetrahydro-2H-benzo[g]indazol-2-yl)thiazolo[4,5-b]quinoxaline (**4e**)

Yellow solid. Yield 40%; m.p. 191~193°C; <sup>1</sup>H NMR (DMSO-*d*<sub>6</sub>, 300 MHz);  $\delta$ : 8.12-8.03 (m, 1H, Ar-H); 7.97 (d,  $J = 7.7$  Hz, 1H, Ar-H); 7.82-7.78 (m, 1H, Ar-H); 7.42-7.30 (m, 2H, Ar-H); 7.33-7.21 (m, 2H, Ar-H); 7.15-7.10 (m, 2H, Ar-H); 7.08-7.01 (m, 1H, Ar-H); 6.95-6.80 (m, 2H, Ar-H); 6.13 (d,  $J = 10.3$  Hz, 1H, CH); 3.57-3.37 (m, 1H, CH); 2.82-2.66 (m, 2H, CH<sub>2</sub>); 2.41 (s, 3H, CH<sub>3</sub>); 1.80-1.73 (m, 1H, CH<sub>2</sub>); 0.85-0.79 (m, 1H, CH<sub>2</sub>). ESI-MS  $m/z$ : 448.2 [M+H]<sup>+</sup>. Anal. Calcd for C<sub>27</sub>H<sub>21</sub>N<sub>5</sub>S (%): C, 72.46; H, 4.73; N, 15.65. Found: C, 72.63; H, 4.69; N, 15.58.

4.2.3.6. 2-(3-(2,4-Dichlorophenyl)-3,3a,4,5-tetrahydro-2H-benzo[g]indazol-2-yl)thiazolo[4,5-b]quinoxaline (**4f**)

White solid. Yield 57%; m.p. 196~198°C; <sup>1</sup>H NMR (DMSO-*d*<sub>6</sub>, 300 MHz); δ: 8.04-7.99 (m, 2H, Ar-H); 7.89-7.81 (m, 2H, Ar-H); 7.74-7.67 (m, 2H, Ar-H); 7.47-7.30 (m, 4H, Ar-H); 7.00 (d, *J* = 8.3 Hz, 1H, CH); 6.41 (d, *J* = 11.3 Hz, 1H, CH); 4.36-4.30 (m, 1H, CH); 3.04-2.87 (m, 2H, CH<sub>2</sub>); 1.94-1.90 (m, 1H, CH<sub>2</sub>); 1.10-1.07 (m, 1H, CH<sub>2</sub>). ESI-MS *m/z*: 502.2 [M+H]<sup>+</sup>. Anal. Calcd for C<sub>26</sub>H<sub>17</sub>Cl<sub>2</sub>N<sub>5</sub>S (%): C, 62.16; H, 3.41; N, 13.94. Found: C, 62.32; H, 3.35; N, 14.04.

4.2.3.7. 2-(3-(3-Chlorophenyl)-3,3a,4,5-tetrahydro-2H-benzo[*g*]indazol-2-yl)thiazolo[4,5-*b*]quinoxaline (**4g**)

Yellow solid. Yield 32%; m.p. 186~187°C; <sup>1</sup>H NMR (DMSO-*d*<sub>6</sub>, 300 MHz); δ: 8.01-7.94 (m, 2H, Ar-H); 7.88-7.82 (m, 1H, Ar-H); 7.70-7.53 (m, 3H, Ar-H); 7.48-7.43 (m, 1H, Ar-H); 7.40-7.32 (m, 3H, Ar-H); 7.30-7.24 (m, 2H, Ar-H); 6.13 (d, *J* = 10.6 Hz, 1H, CH); 4.03-3.98 (m, 1H, CH); 2.95-2.82 (m, 2H, CH<sub>2</sub>); 1.70-1.65 (m, 1H, CH<sub>2</sub>); 0.96-0.90 (m, 1H, CH<sub>2</sub>). ESI-MS *m/z*: 468.3 [M+H]<sup>+</sup>. Anal. Calcd for C<sub>26</sub>H<sub>18</sub>ClN<sub>5</sub>S (%): C, 66.73; H, 3.88; N, 14.97. Found: C, 66.63; H, 3.96; N, 14.86.

4.2.3.8. 2-(3-(2-Chlorophenyl)-3,3a,4,5-tetrahydro-2H-benzo[*g*]indazol-2-yl)thiazolo[4,5-*b*]quinoxaline (**4h**)

Yellow solid. Yield 42%; m.p. 187~189°C; <sup>1</sup>H NMR (DMSO-*d*<sub>6</sub>, 300 MHz); δ: 8.11 (d, *J* = 8.1 Hz, 1H, Ar-H); 8.07-7.95 (m, 2H, Ar-H); 7.72-7.69 (m, 1H, Ar-H); 7.66-7.59 (m, 1H, Ar-H); 7.51 (d, *J* = 7.9 Hz, 1H, Ar-H); 7.43 (d, *J* = 9.1 Hz, 1H, Ar-H); 7.34-7.29 (m, 3H, Ar-H); 7.21-7.13 (m, 2H, Ar-H); 6.20 (d, *J* = 10.5 Hz, 1H, CH); 4.11-4.05 (m, 1H, CH); 2.99-2.83 (m, 2H, CH<sub>2</sub>); 1.85-1.71 (m, 1H, CH<sub>2</sub>); 1.07-1.03 (m, 1H, CH<sub>2</sub>). ESI-MS *m/z*: 468.2 [M+H]<sup>+</sup>. Anal. Calcd for C<sub>26</sub>H<sub>18</sub>ClN<sub>5</sub>S (%): C, 66.73; H, 3.88; N, 14.97. Found: C, 66.62; H, 3.86; N, 16.89.

4.2.3.9. 2-(3-(*M*-tolyl)-3,3a,4,5-tetrahydro-2H-benzo[*g*]indazol-2-yl)thiazolo[4,5-*b*]quinoxaline (**4i**)

Yellow solid. Yield 48%; m.p. 178~180°C; <sup>1</sup>H NMR (DMSO-*d*<sub>6</sub>, 300 MHz); δ: 8.08 (d, *J* = 7.6 Hz, 1H, Ar-H); 7.99 (d, *J* = 8.3 Hz, 1H, Ar-H); 7.82-7.77 (m, 1H, Ar-H); 7.42-7.31 (m, 2H, Ar-H); 7.30-7.21 (m, 2H, Ar-H); 7.15-7.10 (m, 2H, Ar-H); 7.08-7.01 (m, 1H, Ar-H); 6.95-6.80 (m, 2H, Ar-H); 6.13 (d, *J* = 10.2 Hz, 1H, CH); 3.58-3.47 (m, 1H, CH); 2.85-2.76 (m, 2H, CH<sub>2</sub>); 2.48 (s, 3H, CH<sub>3</sub>); 1.80-1.72 (m, 1H, CH<sub>2</sub>); 0.86-0.75 (m, 1H, CH<sub>2</sub>). ESI-MS *m/z*: 448.2 [M+H]<sup>+</sup>. Anal. Calcd for C<sub>27</sub>H<sub>21</sub>N<sub>5</sub>S (%): C, 72.46; H, 4.73; N, 15.65. Found: C, 72.61; H, 4.69; N, 15.58.

4.2.3.10. 2-(3-(*M*-tolyl)-3,3a,4,5-tetrahydro-2H-benzo[*g*]indazol-2-yl)thiazolo[4,5-

b]quinoxaline (**4j**)

White solid. Yield 42%; m.p. 188~190°C; <sup>1</sup>H NMR (DMSO-*d*<sub>6</sub>, 300 MHz); δ: 8.12-7.96 (m, 2H, Ar-H); 7.80 (d, *J* = 7.7 Hz, 1H, Ar-H); 7.35 (d, *J* = 7.6 Hz, 2H, Ar-H); 7.30-7.22 (m, 2H, Ar-H); 7.13-7.10 (m, 2H, Ar-H); 7.08-6.92 (m, 3H, Ar-H); 6.03 (d, *J* = 10.7 Hz, 1H, CH); 3.56-3.41 (m, 1H, CH); 2.82-2.69 (m, 2H, CH<sub>2</sub>); 2.39 (s, 3H, CH<sub>3</sub>); 1.81-1.75 (m, 1H, CH<sub>2</sub>); 0.85-0.73 (m, 1H, CH<sub>2</sub>). ESI-MS *m/z*: 448.2 [M+H]<sup>+</sup>. Anal. Calcd for C<sub>27</sub>H<sub>21</sub>N<sub>5</sub>S (%): C, 72.46; H, 4.73; N, 15.65. Found: C, 72.61; H, 4.66; N, 15.68.

4.2.3.11. 2-(8-Methoxy-3-phenyl-3,3a,4,5-tetrahydro-2H-benzo[*g*]indazol-2-yl)thiazolo[4,5-*b*]quinoxaline (**4k**)

White solid. Yield 43%; m.p. 196~198°C; <sup>1</sup>H NMR (DMSO-*d*<sub>6</sub>, 300 MHz); δ: 7.98 (d, *J* = 6.8 Hz, 1H, Ar-H); 7.84 (d, *J* = 7.3 Hz, 1H, Ar-H); 7.71-7.64 (m, 2H, Ar-H); 7.50-7.42 (m, 1H, Ar-H); 7.34-7.29 (m, 3H, Ar-H); 7.21-7.20 (m, 3H, Ar-H); 7.07-7.05 (m, 1H, Ar-H); 6.16 (d, *J* = 10.7 Hz, 1H, CH); 4.16-4.08 (m, 1H, CH); 3.85 (s, 3H, CH<sub>3</sub>); 2.89-2.81 (m, 2H, CH<sub>2</sub>); 1.85-1.82 (m, 1H, CH<sub>2</sub>); 0.86-0.79 (m, 1H, CH<sub>2</sub>). ESI-MS *m/z*: 464.2 [M+H]<sup>+</sup>. Anal. Calcd for C<sub>27</sub>H<sub>21</sub>N<sub>5</sub>OS (%): C, 69.96; H, 4.57; N, 15.11. Found: C, 69.69; H, 4.49; N, 15.28.

4.2.3.12. 2-(8-Methoxy-3-(4-methoxyphenyl)-3,3a,4,5-tetrahydro-2H-benzo[*g*]indazol-2-yl)thiazolo[4,5-*b*]quinoxaline (**4l**)

White solid. Yield 34%; m.p. 184~186°C; <sup>1</sup>H NMR (DMSO-*d*<sub>6</sub>, 300 MHz); δ: 8.01 (d, *J* = 7.2 Hz, 1H, Ar-H); 7.96 (d, *J* = 7.7 Hz, 1H, Ar-H); 7.86-7.83 (m, 1H, Ar-H); 7.73-7.66 (m, 2H, Ar-H); 7.45-7.34 (m, 2H, Ar-H); 7.31-7.28 (m, 1H, Ar-H); 7.12 (d, *J* = 8.2 Hz, 2H, Ar-H); 6.90 (d, *J* = 8.5 Hz, 1H, Ar-H); 6.11 (d, *J* = 10.6 Hz, 1H, CH); 4.14-4.08 (m, 1H, CH); 3.70 (s, 3H, CH<sub>3</sub>); 3.59 (s, 3H, CH<sub>3</sub>); 3.04-2.83 (m, 2H, CH<sub>2</sub>); 1.84-1.80 (m, 1H, CH<sub>2</sub>); 1.02-0.94 (m, 1H, CH<sub>2</sub>). ESI-MS *m/z*: 494.2 [M+H]<sup>+</sup>. Anal. Calcd for C<sub>28</sub>H<sub>23</sub>N<sub>5</sub>O<sub>2</sub>S (%): C, 68.13; H, 4.70; N, 14.19. Found: C, 68.28; H, 4.59; N, 14.38.

4.2.3.13. 2-(3-(4-Fluorophenyl)-8-methoxy-3,3a,4,5-tetrahydro-2H-benzo[*g*]indazol-2-yl)thiazolo[4,5-*b*]quinoxaline (**4m**)

White solid. Yield 47%; m.p. 181~183°C; <sup>1</sup>H NMR (DMSO-*d*<sub>6</sub>, 300 MHz); δ: 8.10-8.01 (m, 1H, Ar-H); 7.97-7.92 (m, 1H, Ar-H); 7.65 (d, *J* = 2.6 Hz, 1H, Ar-H); 7.55-7.51 (m, 1H, Ar-H); 7.28-7.20 (m, 1H, Ar-H); 7.16-7.09 (m, 3H, Ar-H); 7.04-6.94 (m, 3H, Ar-H); 6.01 (d, *J* = 10.6 Hz, 1H, CH); 3.80 (s, 3H, CH<sub>3</sub>); 3.80-3.67 (m, 1H, CH);

2.81-2.73 (m, 2H, CH<sub>2</sub>); 1.77-1.73 (m, 1H, CH<sub>2</sub>); 0.76-0.61 (m, 1H, CH<sub>2</sub>). ESI-MS m/z: 482.2 [M+H]<sup>+</sup>. Anal. Calcd for C<sub>27</sub>H<sub>20</sub>FN<sub>5</sub>OS (%): C, 67.34; H, 4.19; N, 14.54. Found: C, 67.63; H, 4.29; N, 14.48.

4.2.3.14. 2-(3-(4-Chlorophenyl)-8-methoxy-3,3a,4,5-tetrahydro-2H-benzo[g]indazol-2-yl)thiazolo[4,5-b]quinoxaline (**4n**)

Yellow solid. Yield 33%; m.p. 203~205°C; <sup>1</sup>H NMR (DMSO-*d*<sub>6</sub>, 300 MHz); δ: 8.03-7.91 (m, 2H, Ar-H); 7.88-7.67 (m, 3H, Ar-H); 7.58-7.48 (m, 2H, Ar-H); 7.44-7.38 (m, 1H, Ar-H); 7.35-7.32 (m, 1H, Ar-H); 7.31-7.22 (m, 2H, Ar-H); 6.13 (d, *J* = 10.7 Hz, 1H, CH); 4.12-4.07 (m, 1H, CH); 3.81 (s, 3H, CH<sub>3</sub>); 2.87-2.81 (m, 2H, CH<sub>2</sub>); 1.66-1.61 (m, 1H, CH<sub>2</sub>); 0.95-0.88 (m, 1H, CH<sub>2</sub>). ESI-MS m/z: 498.2 [M+H]<sup>+</sup>. Anal. Calcd for C<sub>27</sub>H<sub>20</sub>ClN<sub>5</sub>OS (%): C, 65.12; H, 4.05; N, 14.06. Found: C, 65.33; H, 4.09; N, 14.28.

4.2.3.15. 2-(8-Methoxy-3-(*p*-tolyl)-3,3a,4,5-tetrahydro-2H-benzo[g]indazol-2-yl)thiazolo[4,5-b]quinoxaline (**4o**)

Yellow solid. Yield 32%; m.p. 202~204°C; <sup>1</sup>H NMR (DMSO-*d*<sub>6</sub>, 300 MHz); δ: 7.92-7.89 (m, 1H, Ar-H); 7.97 (d, *J* = 7.7 Hz, 1H, Ar-H); 7.80 (d, *J* = 8.7 Hz, 1H, Ar-H); 7.35 (d, *J* = 5.4 Hz, 1H, Ar-H); 7.30-7.21 (m, 2H, Ar-H); 7.13-7.07 (m, 2H, Ar-H); 7.05-7.01 (m, 1H, Ar-H); 6.93-6.77 (m, 2H, Ar-H); 6.10 (d, *J* = 10.9 Hz, 1H, CH); 3.81 (s, 3H, CH<sub>3</sub>); 3.57-3.35 (m, 1H, CH); 2.85-2.62 (m, 2H, CH<sub>2</sub>); 2.38 (s, 3H, CH<sub>3</sub>); 1.82-1.71 (m, 1H, CH<sub>2</sub>); 0.88-0.82 (m, 1H, CH<sub>2</sub>). ESI-MS m/z: 478.2 [M+H]<sup>+</sup>. Anal. Calcd for C<sub>28</sub>H<sub>23</sub>N<sub>5</sub>OS (%): C, 70.42; H, 4.85; N, 14.66. Found: C, 70.63; H, 4.59; N, 14.48.

4.2.3.16. 3-Phenyl-2-(thiazolo[4,5-b]quinoxalin-2-yl)-2,3,3a,4-tetrahydrochromeno[4,3-c]pyrazole (**4p**)

White solid. Yield 49%; m.p. 193~195°C; <sup>1</sup>H NMR (DMSO-*d*<sub>6</sub>, 300 MHz); δ: 8.04 (d, *J* = 6.3 Hz, 1H, Ar-H); 7.97 (d, *J* = 7.8 Hz, 1H, Ar-H); 7.88-7.81 (m, 2H, Ar-H); 7.66-7.55 (m, 2H, Ar-H); 7.51-7.37 (m, 3H, Ar-H); 7.30-7.23 (m, 2H, Ar-H); 7.10-6.95 (m, 2H, Ar-H); 5.98 (d, *J* = 10.7 Hz, 1H, CH); 4.63-4.55 (m, 1H, CH); 4.14-4.12 (m, 1H, CH); 4.07-4.03 (m, 1H, CH). ESI-MS m/z: 436.2 [M+H]<sup>+</sup>. Anal. Calcd for C<sub>25</sub>H<sub>17</sub>N<sub>5</sub>OS (%): C, 68.95; H, 3.93; N, 16.08. Found: C, 68.73; H, 3.79; N, 16.28.

4.2.3.17. 3-(4-Methoxyphenyl)-2-(thiazolo[4,5-b]quinoxalin-2-yl)-2,3,3a,4-tetrahydrochromeno[4,3-c]pyrazole (**4q**)

White solid. Yield 43%; m.p. 207~209°C; <sup>1</sup>H NMR (DMSO-*d*<sub>6</sub>, 300 MHz); δ: 8.03

(d,  $J = 7.3$  Hz, 1H, Ar-H); 7.97 (d,  $J = 7.5$  Hz, 1H, Ar-H); 7.86-7.74 (m, 3H, Ar-H); 7.46-7.34 (m, 2H, Ar-H); 7.32-7.25 (m, 1H, Ar-H); 7.12-6.99 (m, 4H, Ar-H); 6.20 (d,  $J = 10.4$  Hz, 1H, CH); 4.44-4.41 (m, 1H, CH<sub>2</sub>); 4.24-4.12 (m, 1H, CH); 3.86-3.76 (m, 1H, CH<sub>2</sub>); 3.78 (s, 3H, CH<sub>3</sub>). ESI-MS  $m/z$ : 466.2 [M+H]<sup>+</sup>. Anal. Calcd for C<sub>26</sub>H<sub>19</sub>N<sub>5</sub>O<sub>2</sub>S (%): C, 67.08; H, 4.11; N, 15.04. Found: C, 67.32; H, 4.22; N, 15.15.

4.2.3.18. 3-(4-Fluorophenyl)-2-(thiazolo[4,5-b]quinoxalin-2-yl)-2,3,3a,4-tetrahydrochromeno[4,3-c]pyrazole (**4r**)

White solid. Yield 37%; m.p. 211~213 °C; <sup>1</sup>H NMR (DMSO-*d*<sub>6</sub>, 300 MHz);  $\delta$ : 8.06 (d,  $J = 7.3$  Hz, 1H, Ar-H); 7.99-7.97 (m, 1H, Ar-H); 7.82-7.76 (m, 1H, Ar-H); 7.40-7.33 (m, 1H, Ar-H); 7.30-7.28 (m, 2H, Ar-H); 7.23-7.20 (m, 1H, Ar-H); 7.15-7.09 (m, 3H, Ar-H); 7.05-7.00 (m, 2H, Ar-H); 6.02 (d,  $J = 10.9$  Hz, 1H, CH); 4.66-4.58 (m, 1H, CH<sub>2</sub>), 4.11-4.08 (m, 1H, CH<sub>2</sub>); 3.87-3.37 (m, 1H, CH). ESI-MS  $m/z$ : 454.2 [M+H]<sup>+</sup>. Anal. Calcd for C<sub>25</sub>H<sub>16</sub>FN<sub>5</sub>OS (%): C, 66.21; H, 3.56; N, 15.44. Found: C, 66.53; H, 3.49; N, 15.53.

4.2.3.19. 3-(4-Chlorophenyl)-2-(thiazolo[4,5-b]quinoxalin-2-yl)-2,3,3a,4-tetrahydrochromeno[4,3-c]pyrazole (**4s**)

Yellow solid. Yield 31%; m.p. 174~176 °C; <sup>1</sup>H NMR (DMSO-*d*<sub>6</sub>, 300 MHz);  $\delta$ : 8.01-7.95 (m, 2H, Ar-H); 7.88-7.82 (m, 1H, Ar-H); 7.720-7.66 (m, 2H, Ar-H); 7.54-7.49 (m, 2H, Ar-H); 7.43-7.37 (m, 3H, Ar-H); 7.31-7.25 (m, 2H, Ar-H); 6.07 (d,  $J = 10.1$  Hz, 1H, CH); 4.41-4.33 (dd,  $J = 10.1$  and 12.2 Hz, 1H, CH<sub>2</sub>); 4.06-3.97 (m, 1H, CH); 3.89-3.77 (dd,  $J = 6.1$  and 10.2 Hz, 1H, CH<sub>2</sub>). ESI-MS  $m/z$ : 470.1 [M+H]<sup>+</sup>. Anal. Calcd for C<sub>25</sub>H<sub>16</sub>ClN<sub>5</sub>OS (%): C, 63.89; H, 3.43; N, 14.90. Found: C, 63.63; H, 3.49; N, 14.78.

4.2.3.20. 2-(Thiazolo[4,5-b]quinoxalin-2-yl)-3-(*p*-tolyl)-2,3,3a,4-tetrahydrochromeno[4,3-c]pyrazole (**4t**)

Yellow solid. Yield 32%; m.p. 197~199 °C; <sup>1</sup>H NMR (DMSO-*d*<sub>6</sub>, 300 MHz);  $\delta$ : 8.10 (d,  $J = 7.7$  Hz, 1H, Ar-H); 7.97 (d,  $J = 4.4$  Hz, 1H, Ar-H); 7.82-7.78 (m, 1H, Ar-H); 7.42-7.22 (m, 4H, Ar-H); 7.13-7.09 (m, 2H, Ar-H); 7.03-6.93 (m, 3H, Ar-H); 6.33 (d,  $J = 10.6$  Hz, 1H, CH); 4.42-4.37 (m, 1H, CH<sub>2</sub>); 3.88-3.78 (m, 1H, CH<sub>2</sub>); 3.47-3.37 (m, 1H, CH); 2.41 (s, 3H, CH<sub>3</sub>). ESI-MS  $m/z$ : 450.2 [M+H]<sup>+</sup>. Anal. Calcd for C<sub>26</sub>H<sub>19</sub>N<sub>5</sub>OS (%): C, 69.47; H, 4.26; N, 15.58. Found: C, 69.63; H, 4.39; N, 15.48.

4.2.3.21. 8-Methyl-3-phenyl-2-(thiazolo[4,5-b]quinoxalin-2-yl)-2,3,3a,4-tetrahydrochromeno[4,3-c]pyrazole (**4u**)

White solid. Yield 42%; m.p. 187~189°C;  $^1\text{H}$  NMR (DMSO- $d_6$ , 300 MHz);  $\delta$ : 7.99 (d,  $J = 8.7$  Hz, 2H, Ar-H); 7.82-7.77 (d,  $J = 6.7$  Hz, 1H, Ar-H); 7.42-7.21 (m, 4H, Ar-H); 7.16-7.11 (m, 2H, Ar-H); 7.08-7.03 (m, 1H, Ar-H); 6.93-6.83 (m, 2H, Ar-H); 6.03 (d,  $J = 10.1$  Hz, 1H, CH); 4.51-4.42 (m, 1H, CH<sub>2</sub>); 3.80-3.77 (m, 1H, CH<sub>2</sub>); 3.55-3.43 (m, 1H, CH); 2.48 (s, 3H, CH<sub>3</sub>). ESI-MS  $m/z$ : 450.2 [M+H]<sup>+</sup>. Anal. Calcd for C<sub>26</sub>H<sub>19</sub>N<sub>5</sub>OS (%): C, 69.47; H, 4.26; N, 15.58. Found: C, 69.63; H, 4.33; N, 15.48.

4.2.3.22. 3-(4-Methoxyphenyl)-8-methyl-2-(thiazolo[4,5-b]quinoxalin-2-yl)-2,3,3a,4-tetrahydrochromeno[4,3-c]pyrazole (**4v**)

Yellow solid. Yield 36%; m.p. 192~194°C;  $^1\text{H}$  NMR (DMSO- $d_6$ , 300 MHz);  $\delta$ : 8.02-7.95 (m, 1H, Ar-H); 7.88-7.82 (m, 1H, Ar-H); 7.77 (d,  $J = 8.7$  Hz, 1H, Ar-H); 7.45-7.30 (m, 3H, Ar-H); 7.22-7.17 (m, 2H, Ar-H); 7.10-6.88 (m, 3H, Ar-H); 6.25 (d,  $J = 10.4$  Hz, 1H, CH); 4.44-4.33 (dd,  $J = 10.3$  and 12.8 Hz, 1H, CH<sub>2</sub>); 3.81 (s, 3H, CH<sub>3</sub>); 3.65-3.59 (dd,  $J = 6.0$  and 10.2 Hz, 1H, CH<sub>2</sub>); 3.55-3.42 (m, 1H, CH); 2.33 (s, 3H, CH<sub>3</sub>). ESI-MS  $m/z$ : 480.2 [M+H]<sup>+</sup>. Anal. Calcd for C<sub>27</sub>H<sub>21</sub>N<sub>5</sub>O<sub>2</sub>S (%): C, 67.62; H, 4.41; N, 14.60. Found: C, 67.38; H, 4.49; N, 14.48.

4.2.3.23. 3-(4-Fluorophenyl)-8-methyl-2-(thiazolo[4,5-b]quinoxalin-2-yl)-2,3,3a,4-tetrahydrochromeno[4,3-c]pyrazole (**4w**)

White solid. Yield 42%; m.p. 199~201°C;  $^1\text{H}$  NMR (DMSO- $d_6$ , 300 MHz);  $\delta$ : 8.12-8.01 (m, 1H, Ar-H); 7.96-7.92 (m, 1H, Ar-H); 7.62 (d,  $J = 3.6$  Hz, 1H, Ar-H); 7.54-7.50 (m, 1H, Ar-H); 7.28-7.21 (m, 1H, Ar-H); 7.16-7.09 (m, 3H, Ar-H); 7.04-6.94 (m, 3H, Ar-H); 6.06 (d,  $J = 10.9$  Hz, 1H, CH); 4.55-4.49 (dd,  $J = 11.1$  and 13.2 Hz, 1H, CH<sub>2</sub>); 3.80-3.69 (m, 1H, CH); 3.55-3.49 (dd,  $J = 5.1$  and 10.2 Hz, 1H, CH<sub>2</sub>); 2.34 (s, 3H, CH<sub>3</sub>). ESI-MS  $m/z$ : 468.2 [M+H]<sup>+</sup>. Anal. Calcd for C<sub>26</sub>H<sub>18</sub>FN<sub>5</sub>OS (%): C, 66.79; H, 3.88; N, 14.98. Found: C, 66.63; H, 3.79; N, 14.73.

4.2.3.24. 3-(4-Chlorophenyl)-8-methyl-2-(thiazolo[4,5-b]quinoxalin-2-yl)-2,3,3a,4-tetrahydrochromeno[4,3-c]pyrazole (**4x**)

White solid. Yield 51%; m.p. 205~207°C;  $^1\text{H}$  NMR (DMSO- $d_6$ , 300 MHz);  $\delta$ : 8.04-7.96 (m, 2H, Ar-H); 7.85-7.80 (m, 2H, Ar-H); 7.75-7.63 (m, 2H, Ar-H); 7.47-7.30 (m, 4H, Ar-H); 6.94 (d,  $J = 8.3$  Hz, 1H, CH); 6.31 (d,  $J = 10.2$  Hz, 1H, CH); 4.60-4.51 (m, 1H, CH<sub>2</sub>); 4.26-4.20 (m, 1H, CH); 3.88-3.79 (m, 1H, CH<sub>2</sub>); 2.41 (s, 3H, CH<sub>3</sub>). ESI-MS  $m/z$ : 484.1 [M+H]<sup>+</sup>. Anal. Calcd for C<sub>26</sub>H<sub>18</sub>ClN<sub>5</sub>OS (%): C, 64.52; H, 3.75; N, 14.47. Found: C, 64.63; H, 3.59; N, 14.38.

4.2.3.25. 8-Methyl-2-(thiazolo[4,5-b]quinoxalin-2-yl)-3-(p-tolyl)-2,3,3a,4-

tetrahydrochromeno[4,3-c]pyrazole (**4y**)

Yellow solid. Yield 43%; m.p. 196~198 °C; <sup>1</sup>H NMR (DMSO-*d*<sub>6</sub>, 300 MHz); δ: 8.03 (d, *J* = 7.2 Hz, 1H, Ar-H); 7.92 (d, *J* = 7.3 Hz, 1H, Ar-H); 7.82-7.72 (m, 1H, Ar-H); 7.42-7.21 (m, 4H, Ar-H); 7.13-7.02 (m, 2H, Ar-H); 6.92-6.80 (m, 2H, Ar-H); 6.19 (d, *J* = 10.8 Hz, 1H, CH); 4.49-4.39 (dd, *J* = 10.3 and 12.8 Hz, 1H, CH<sub>2</sub>); 3.77-3.69 (dd, *J* = 5.1 and 10.2 Hz, 1H, CH<sub>2</sub>); 3.53-3.44 (m, 1H, CH); 2.48 (s, 3H, CH<sub>3</sub>); 2.44 (s, 3H, CH<sub>3</sub>). ESI-MS *m/z*: 464.2 [M+H]<sup>+</sup>. Anal. Calcd for C<sub>27</sub>H<sub>21</sub>N<sub>5</sub>OS (%): C, 69.96; H, 4.57; N, 15.11. Found: C, 69.63; H, 4.49; N, 15.28.

### 4.3 Preparation, purification of EGFR and HER-2 and inhibitory assay

A 1.6 kb cDNA encoded for the EGFR cytoplasmic domain (EGFR-CD, amino acids 645–1186) and 1.7 Kb cDNA encoded for human HER-2 cytoplasmic domain (HER-2-CD, amino acids 676–1245) were cloned into baculoviral expression vectors pBlueBacHis2B and pFASTBacHTc (Huakang Company, China), separately. A sequence that encodes (His)<sub>6</sub> was located at the 5' upstream to the EGFR and HER-2 sequences. Sf-9 cells were infected for 3 days for protein expression. Sf-9 cell pellets were solubilized at 0 °C in a buffer at pH 7.4 containing 50 mM HEPES, 10 mM NaCl, 1% Triton, 10 μM ammonium molybdate, 100 μM sodium vanadate, 10 μg/mL aprotinin, 10 μg/mL leupeptin, 10 μg/mL pepstatin, and 16 μg/mL benzamidine HCl for 20 min followed by 20 min centrifugation. Crude extract supernatant was passed through an equilibrated Ni-NTA superflow packed column and washed with 10 mM and then 100 mM imidazole to remove nonspecifically bound material. Histidine tagged proteins were eluted with 250 and 500 mM imidazole and dialyzed against 50 mM NaCl, 20 mM HEPES, 10% glycerol, and 1 μg/mL each of aprotinin, leupeptin, and pepstatin for 2 h. The entire purification procedure was performed at 4 °C or on ice.

Both EGFR and HER-2 kinase assays were set up to assess the level of autophosphorylation based on DELFIA/Time-Resolved Fluorometry. Compounds **4a-4y** were dissolved in 100% DMSO and diluted to the appropriate concentrations with 25 mM HEPES at pH 7.4. In each well, 10 μL compound was incubated with 10 μL (12.5 ng for HER-2 or 5 ng for EGFR) recombinant enzyme (1:80 dilution in 100 mM HEPES) for 10 min at room temperature. Then, 10 μL of 5 mM buffer (containing 20 mM HEPES, 2 mM MnCl<sub>2</sub>, 100 μM Na<sub>3</sub>VO<sub>4</sub>, and 1 mM DTT) and 20 μL of 0.1 mM ATP–50 mM MgCl<sub>2</sub> were added for 1 h. Positive and negative controls were included

in each plate by incubation of enzyme with or without ATP–MgCl<sub>2</sub>. At the end of incubation, liquid was aspirated, and plates were washed three times with wash buffer. A 75 μL (400 ng) sample of europium labeled anti-phosphotyrosine antibody was added to each well for another 1 h of incubation. After washing, enhancement solution was added and the signal was detected by Victor (Wallac Inc.) with excitation at 340 nm and emission at 615 nm. The percentage of auto-phosphorylation inhibition by the compounds was calculated using the following formula: 100% - [(negative control)/(positive control - negative control)]. The IC<sub>50</sub> was obtained from curves of percentage inhibition with eight concentrations of compound. As the contaminants in the enzyme preparation are fairly low, the majority of the signal detected by the anti-phosphotyrosine antibody is from EGFR or HER-2.

#### 4.4 Antiproliferative activity

The antiproliferative activities of the prepared compounds were evaluated using a standard (MTT)-based colorimetric assay with some modification. Cell lines were grown to log phase in DMEM supplemented with 10% fetal bovine serum, under a humidified atmosphere of 5% CO<sub>2</sub> at 37 °C. Cell suspensions were prepared and 100 μL/well dispensed into 96-well plates giving 10<sup>5</sup> cells/well. The plates were returned to the incubator for 24 h to allow the cells to reattach. Subsequently, cells were treated with the target compounds at increasing concentrations in the presence of 10% FBS for 48 h. Then, cell viability was assessed by the conventional 3-(4, 5-dimethylthiazol-2-yl)-2,5-diphenyltetrazolium bromide (MTT) reduction assay and carried out strictly according to the manufacturer instructions (Sigma). The absorbance (OD<sub>570</sub>) was read on an ELISA reader (Tecan, Austria).

#### 4.5 Experimental protocol of docking study

Molecular docking of compounds **4l** and **4x** into the three dimensional X-ray structure of EGFR (PDB code: 1M17) were carried out using the Discovery Studio (version 3.5) as implemented through the graphical user interface DS-CDOCKER protocol. The three-dimensional structures of the aforementioned compounds were constructed using Chem. 3D ultra 12.0 software [Chemical Structure Drawing Standard; Cambridge Soft corporation, USA (2013)], then they were energetically minimized by using MMFF94 with 5000 iterations and minimum RMS gradient of 0.10. The crystal structures of protein complex were retrieved from the RCSB Protein Data Bank (<http://www.rcsb.org/pdb/home/home.do>). All bound waters and ligands

were eliminated from the protein. The molecular docking was performed by inserting compounds **4l** and **4x** into the binding pocket of EGFR based on the binding mode. Types of interactions of the docked protein with ligand-based pharmacophore model were analyzed after the end of molecular docking.

#### 4.6. 3D-QSAR

Ligand-based 3D-QSAR approach was performed by QSAR software of DS 3.5 (Discovery Studio 3.5, Accelrys, Co.Ltd). The training sets were composed of inhibitors with the corresponding pIC<sub>50</sub> values which were converted from the obtained IC<sub>50</sub> ( $\mu$ M), and test sets comprised compounds of data sets as list in **Table 4**.

All the definition of the descriptors can be seen in the “Help” of DS 3.5 software and they were calculated by QSAR protocol of DS 3.5. The alignment conformation of each molecule was the one with lowest interaction energy in the docked results of CDOCKER. The predictive ability of 3D-QSAR modeling can be evaluated based on the cross-validated correlation coefficient, which qualifies the predictive ability of the models. Scrambled test (Y scrambling) was performed to investigate the risk of chance correlations. The inhibitory potencies of compounds were randomly reordered for 30 times and subject to leave-one-out validation test, respectively. The models were also validated by test sets, in which the compounds are not included in the training sets.

#### Acknowledgement

This work is supported by The Fundamental Research Funds for the Central Universities (2242014R30019), Technology Supporting Program of Jiangsu province (BE2012657), and National Basin Research Program of China (No. 2011CB933503). We thank Pro. Hai-liang Zhu (State Key Laboratory of Pharmaceutical Biotechnology, Nanjing University) for a license to use their software.

#### References and notes

1. A. S. El-Azab, M. A. Al-Omar, A. A. Abdel-Aziz, N. I. Abdel-Aziz, M. A. el-Sayed, A. M. Aleisa, M. M. Sayed-Ahmed and S. G. Abdel-Hamide, *European journal of medicinal chemistry*, 2010, **45**, 4188-4198.
2. L. Seymour, *Cancer treatment reviews*, 1999, **25**, 301-312.
3. J. D. Jordan, E. M. Landau and R. Iyengar, *Cell*, 2000, **103**, 193-200.
4. S. K. Rabindran, D. D. Ross, L. A. Doyle, W. Yang and L. M. Greenberger, *Cancer Res*, 2000, **60**, 47-50.
5. D. M. Shin, F. R. Khuri, B. S. Glisson, L. Ginsberg, V. M. Papadimitrakopoulou, G. Clayman, J. J. Lee, K. K. Ang, S. M. Lippman and W. K. Hong, *Cancer*, 2001, **91**, 1316-1323.
6. P. Cohen, *Nature reviews. Drug discovery*, 2002, **1**, 309-315.

7. A. Levitzki, *Accounts of chemical research*, 2003, **36**, 462-469.
8. A. A. Adjei, *Journal of the National Cancer Institute*, 2001, **93**, 1062-1074.
9. X. W. Zhang, J. Gureasko, K. Shen, P. A. Cole and J. Kuriyan, *Cell*, 2006, **125**, 1137-1149.
10. S. Guo, L. S. Colbert, M. Fuller, Y. Zhang and R. R. Gonzalez-Perez, *Biochimica et biophysica acta*, 2010, **1806**, 108-121.
11. K. S. Kolibaba and B. J. Druker, *Biochimica et biophysica acta*, 1997, 1333, F217-248.
12. P. Traxler, *Expert opinion on therapeutic targets*, 2003, **7**, 215-234.
13. S. S. Sridhar, L. Seymour and F. A. Shepherd, *The Lancet. Oncology*, 2003, **4**, 397-406.
14. J. Vansteenkiste, *Expert review of anticancer therapy*, 2004, **4**, 5-17.
15. S. Madhusudan and T. S. Ganesan, *Clinical biochemistry*, 2004, **37**, 618-635.
16. C. Y. Hsieh, P. C. Tsai, C. H. Tseng, Y. L. Chen, L. S. Chang and S. R. Lin, *Toxicology in vitro : an international journal published in association with BIBRA*, 2013, **27**, 1-10.
17. Y. Y. Xu, Y. Cao, H. Ma, H. Q. Li and G. Z. Ao, *Bioorganic & medicinal chemistry*, 2013, **21**, 388-394.
18. N. C. Valerie, B. Dziegielewska, A. S. Hosing, E. Augustin, L. S. Gray, D. L. Brautigan, J. M. Larner and J. Dziegielewski, *Biochemical pharmacology*, 2013, **85**, 888-897.
19. A. J. Bridges, *Curr Med Chem*, 1999, **6**, 825-843.
20. S. Manfredini, R. Bazzanini, P. G. Baraldi, M. Guarneri, D. Simoni, M. E. Marongiu, A. Pani, E. Tramontano and P. La Colla, *Journal of medicinal chemistry*, 1992, **35**, 917-924.
21. S. Manfredini, R. Bazzanini, P. G. Baraldi, M. Bonora, M. Marangoni, D. Simoni, A. Pani, F. Scintu, E. Pinna, L. Pisano and P. La Colla, *Anti-cancer drug design*, 1996, **11**, 193-204.
22. H. J. Park, K. Lee, S. J. Park, B. Ahn, J. C. Lee, H. Cho and K. I. Lee, *Bioorganic & medicinal chemistry letters*, 2005, **15**, 3307-3312.
23. A. Tanitame, Y. Oyamada, K. Ofuji, M. Fujimoto, N. Iwai, Y. Hiyama, K. Suzuki, H. Ito, H. Terauchi, M. Kawasaki, K. Nagai, M. Wachi and J. Yamagishi, *Journal of medicinal chemistry*, 2004, **47**, 3693-3696.
24. S. Guniz Kucukguzel, S. Rollas, H. Erdeniz, M. Kiraz, A. Cevdet Ekinici and A. Vidin, *European journal of medicinal chemistry*, 2000, **35**, 761-771.
25. T. D. Penning, J. J. Talley, S. R. Bertenshaw, J. S. Carter, P. W. Collins, S. Docter, M. J. Graneto, L. F. Lee, J. W. Malecha, J. M. Miyashiro, R. S. Rogers, D. J. Rogier, S. S. Yu, AndersonGd, E. G. Burton, J. N. Cogburn, S. A. Gregory, C. M. Koboldt, W. E. Perkins, K. Seibert, A. W. Veenhuizen, Y. Y. Zhang and P. C. Isakson, *Journal of medicinal chemistry*, 1997, **40**, 1347-1365.
26. G. Menozzi, L. Mosti, P. Fossa, F. Mattioli and M. Ghia, *J Heterocyclic Chem*, 1997, **34**, 963-968.
27. R. Sridhar, P. T. Perumal, S. Etti, G. Shanmugam, M. N. Ponnuswamy, V. R. Prabavathy and N. Mathivanan, *Bioorganic & medicinal chemistry letters*, 2004, **14**, 6035-6040.
28. G. R. Bebernitz, G. Argentieri, B. Battle, C. Brennan, B. Balkan, B. F. Burkey, M. Eckhardt, J. Gao, P. Kapa, R. J. Strohschein, H. F. Schuster, M. Wilson and D. D. Xu, *Journal of medicinal chemistry*, 2001, **44**, 2601-2611.
29. P. C. Lv, H. Q. Li, J. Sun, Y. Zhou and H. L. Zhu, *Bioorganic & medicinal chemistry*, 2010, **18**, 4606-4614.
30. P. C. Lv, D. D. Li, Q. S. Li, X. Lu, Z. P. Xiao and H. L. Zhu, *Bioorganic & medicinal chemistry letters*, 2011, **21**, 5374-5377.
31. K. M. Qiu, H. H. Wang, L. M. Wang, Y. Luo, X. H. Yang, X. M. Wang and H. L. Zhu, *Bioorganic & medicinal chemistry*, 2012, **20**, 2010-2018.
32. P. Corona, A. Carta, M. Loriga, G. Vitale and G. Paglietti, *European journal of medicinal chemistry*, 2009, **44**, 1579-1591.
33. F. A. Rodrigues, S. Bomfim Ida, B. C. Cavalcanti, O. Pessoa Cdo, J. L. Wardell, S. M. Wardell, A. C. Pinheiro, C. R. Kaiser, T. C. Nogueira, J. N. Low, L. R. Gomes and M. V. de Souza, *Bioorganic & medicinal chemistry letters*, 2014, **24**, 934-939.
34. T. R. Mielcke, A. Mascarello, E. Filippi-Chiela, R. F. Zanin, G. Lenz, P. C. Leal, L. D. Chirardia, R. A. Yunes, R. J. Nunes, A. M. O. Battastini, F. B. Morrone and M. M. Campos, *European journal of medicinal chemistry*, 2012, **48**, 255-264.
35. J. Stamos, M. X. Sliwowski and C. Eigenbrot, *The Journal of biological chemistry*, 2002, **277**, 46265-46272.
36. W. J. Egan, K. M. Merz, Jr. and J. J. Baldwin, *Journal of medicinal chemistry*, 2000, **43**, 3867-3877.

### Figure Captions

**Table 1** *In vitro* antiproliferative activities ( $IC_{50}$ ,  $\mu M$ ) of compound **4a-4y** against four human tumor cell lines

**Table 2.** Enzyme inhibition activities of compounds **4a-4y** against EGFR and HER-2

**Table 3.** The median cytotoxic concentration ( $CC_{50}$ ) data of all compounds.

**Table 4.** Experimental, predicted inhibitory activity of compounds **4a-4y** against EGFR protein by 3D-QSAR model

**Fig. 1** Chemical structures of EGFR and HER-2 inhibitors

**Fig. 2** Design strategy and modification of novel EGFR/HER-2 inhibitors.

**Fig. 3** Docking modes of compounds in the binding pockets of EGFR (PDB ID: 1M17). Interactions between the protein and the ligand are shown as yellow dotted lines, the residues are shown as orange sticks, and the ligands are shown as stick models in green (**4l**), cyan (**4x**) and magenta (**Erlotinib**): **(A)** Predicted binding mode of **4l** with EGFR; **(B)** The surface of binding site of **4l** with EGFR; **(C)** Predicted binding mode of **4x** with EGFR; **(D)** The surface of binding site of **4x** with EGFR; **(E)** Predicted binding mode of **Erlotinib** with EGFR; **(F)** The docking modes of compound **4l**, **4x** and **Erlotinib** in the active site of EGFR.

**Fig. 4** Plot of experimental vs. predicted EGFR inhibitory activities of training set and test set.

**Fig. 5** (a) 3D QSAR model coefficients on electrostatic potential grids. Blue represents positive coefficients; red represents negative coefficients. (b) 3D QSAR model coefficients on van der Waals grids. Green represents positive coefficients; yellow represents negative coefficients.

**Scheme 1.** Synthetic route for the preparation of the target compounds **4a-4y**. Reagents and conditions: (a) ArCHO, 8 N NaOH, ethanol, 2 h, r.t. 65-83%; (b) thiosemicarbazide, NaOH, ethanol, 8 h, reflux, 62-75%; (c) 2,3-dichloroquinoxaline, ethanol, 8 h, reflux, 31-57%.

**Table 1** *In vitro* antiproliferative activities (IC<sub>50</sub>, μM) of compound **4a-4y** against four human tumor cell lines

Compounds	R <sub>1</sub>	R <sub>2</sub>	X	IC <sub>50</sub> (μM) <sup>a</sup>			
				A549	MCF-7	Hela	HepG2
<b>4a</b>	H	H	C	8.32	6.88	2.98	4.38
<b>4b</b>	H	4-OCH <sub>3</sub>	C	4.38	3.28	8.25	2.58
<b>4c</b>	H	4-F	C	28.26	15.26	5.38	10.08
<b>4d</b>	H	4-Cl	C	15.26	11.33	15.24	17.18
<b>4e</b>	H	4-CH <sub>3</sub>	C	4.62	5.86	8.89	5.58
<b>4f</b>	H	2,4-Cl	C	15.34	28.26	12.25	19.56
<b>4g</b>	H	3-Cl	C	15.26	18.26	9.28	10.08
<b>4h</b>	H	2-Cl	C	8.88	8.23	10.33	5.36
<b>4i</b>	H	3-CH <sub>3</sub>	C	15.36	10.16	16.28	8.99
<b>4j</b>	H	2-CH <sub>3</sub>	C	13.22	14.87	18.27	19.23
<b>4k</b>	OCH <sub>3</sub>	H	C	5.38	3.48	6.28	4.18
<b>4l</b>	OCH <sub>3</sub>	4-OCH <sub>3</sub>	C	3.04	1.91	7.38	5.76
<b>4m</b>	OCH <sub>3</sub>	4-F	C	14.19	12.28	10.25	12.61
<b>4n</b>	OCH <sub>3</sub>	4-Cl	C	24.73	8.23	7.46	15.25
<b>4o</b>	OCH <sub>3</sub>	4-CH <sub>3</sub>	C	9.59	2.53	16.23	14.57
<b>4p</b>	H	H	O	4.12	6.83	5.88	12.56
<b>4q</b>	H	4-OCH <sub>3</sub>	O	4.26	3.23	7.63	6.12
<b>4r</b>	H	4-F	O	10.92	28.22	15.66	18.59
<b>4s</b>	H	4-Cl	O	24.96	13.36	31.54	9.88
<b>4t</b>	H	4-CH <sub>3</sub>	O	6.82	3.99	6.81	7.26
<b>4u</b>	CH <sub>3</sub>	H	O	4.47	12.8	2.02	8.29
<b>4v</b>	CH <sub>3</sub>	4-OCH <sub>3</sub>	O	6.38	2.02	5.38	5.66
<b>4w</b>	CH <sub>3</sub>	4-F	O	18.65	21.34	26.98	24.45
<b>4x</b>	CH <sub>3</sub>	4-Cl	O	28.26	16.26	17.64	17.05
<b>4y</b>	CH <sub>3</sub>	4-CH <sub>3</sub>	O	13.67	3.28	7.46	11.38
<b>Erlotinib</b>				4.28	2.32	1.93	3.02
<b>Gefitinib</b>				2.96	6.26	4.12	3.18

<sup>a</sup> Antiproliferation activity was measured using the MTT assay. Values are the average of three independent experiments run in triplicate. Variation was generally 5-10%.

**Table 2.** Enzyme inhibition activities of compounds **4a-4y** against EGFR and HER-2

Compounds	IC <sub>50</sub> (μM) <sup>a</sup>		Compounds	IC <sub>50</sub> (μM) <sup>a</sup>	
	EGFR <sup>b</sup>	HER-2 <sup>b</sup>		EGFR <sup>b</sup>	HER-2 <sup>b</sup>
<b>4a</b>	9.82	11.43	<b>4n</b>	18.23	25.46
<b>4b</b>	2.26	3.68	<b>4o</b>	0.96	3.23
<b>4c</b>	21.24	18.43	<b>4p</b>	3.32	8.68

<b>4d</b>	15.67	26.58	<b>4q</b>	1.23	5.25
<b>4e</b>	8.26	12.38	<b>4r</b>	18.26	30.46
<b>4f</b>	15.83	17.46	<b>4s</b>	15.34	28.4
<b>4g</b>	14.63	11.06	<b>4t</b>	2.36	5.67
<b>4h</b>	15.82	3.04	<b>4u</b>	5.23	11.34
<b>4i</b>	9.26	13.98	<b>4v</b>	0.86	2.35
<b>4j</b>	15.28	20.88	<b>4w</b>	15.28	33.56
<b>4k</b>	4.68	5.34	<b>4x</b>	6.8	12.8
<b>4l</b>	0.28	1.26	<b>4y</b>	1.23	4.66
<b>4m</b>	8.16	15.24	<b>Erlotinib</b>	0.08	0.23

<sup>a</sup> Errors were in the range of 5-10% of the reported values, from three different assays.

<sup>b</sup> Human recombinant enzymes, by the esterase assay (4-nitrophenylacetate as substrate).

**Table 3.** The median cytotoxic concentration (CC<sub>50</sub>) data of all compounds.

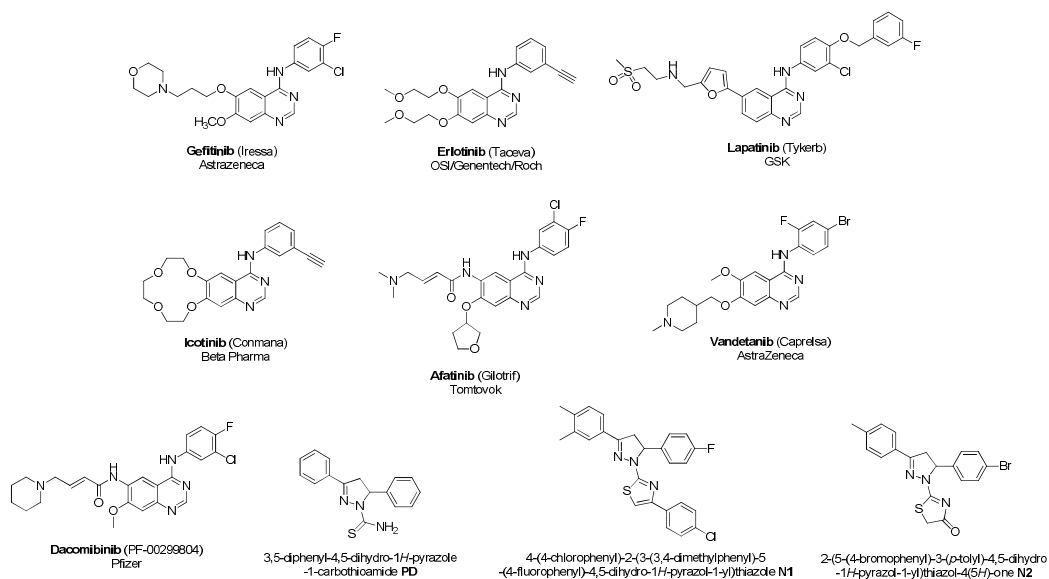
Compounds	CC <sub>50</sub> , μmol <sup>a</sup>	Compounds	CC <sub>50</sub> , μmol <sup>a</sup>
<b>4a</b>	51.28	<b>4n</b>	51.42
<b>4b</b>	55.43	<b>4o</b>	68.45
<b>4c</b>	46.78	<b>4p</b>	48.28
<b>4d</b>	50.36	<b>4q</b>	56.12
<b>4e</b>	53.28	<b>4r</b>	41.56
<b>4f</b>	55.33	<b>4s</b>	48.33
<b>4g</b>	46.72	<b>4t</b>	52.67
<b>4h</b>	49.38	<b>4u</b>	48.16
<b>4i</b>	52.68	<b>4v</b>	59.26
<b>4j</b>	51.47	<b>4w</b>	51.38
<b>4k</b>	61.33	<b>4x</b>	48.34
<b>4l</b>	78.44	<b>4y</b>	56.25
<b>4m</b>	55.56	<b>Erlotinib</b>	68.03

<sup>a</sup> The cytotoxicity of each compound was expressed as the concentration of compound that reduced cell viability to 50% (CC<sub>50</sub>).

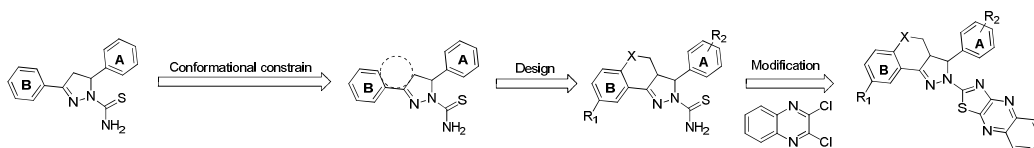
**Table 4.** Experimental, predicted inhibitory activity of compounds **4a-4y** against EGFR protein by 3D-QSAR model

Compo unds	EGFR		Compo unds	EGFR	
	Actual-pIC <sub>50</sub>	Preticted- pIC <sub>50</sub>		Actual-pIC <sub>50</sub>	Preticted- pIC <sub>50</sub>
<b>4a</b>	5.01	5.08	<b>4n</b>	4.74	4.92
<b>4b</b>	5.65	5.70	<b>4o</b>	6.02	6.01
<b>4c</b>	4.67	4.56	<b>4p</b>	5.48	5.41

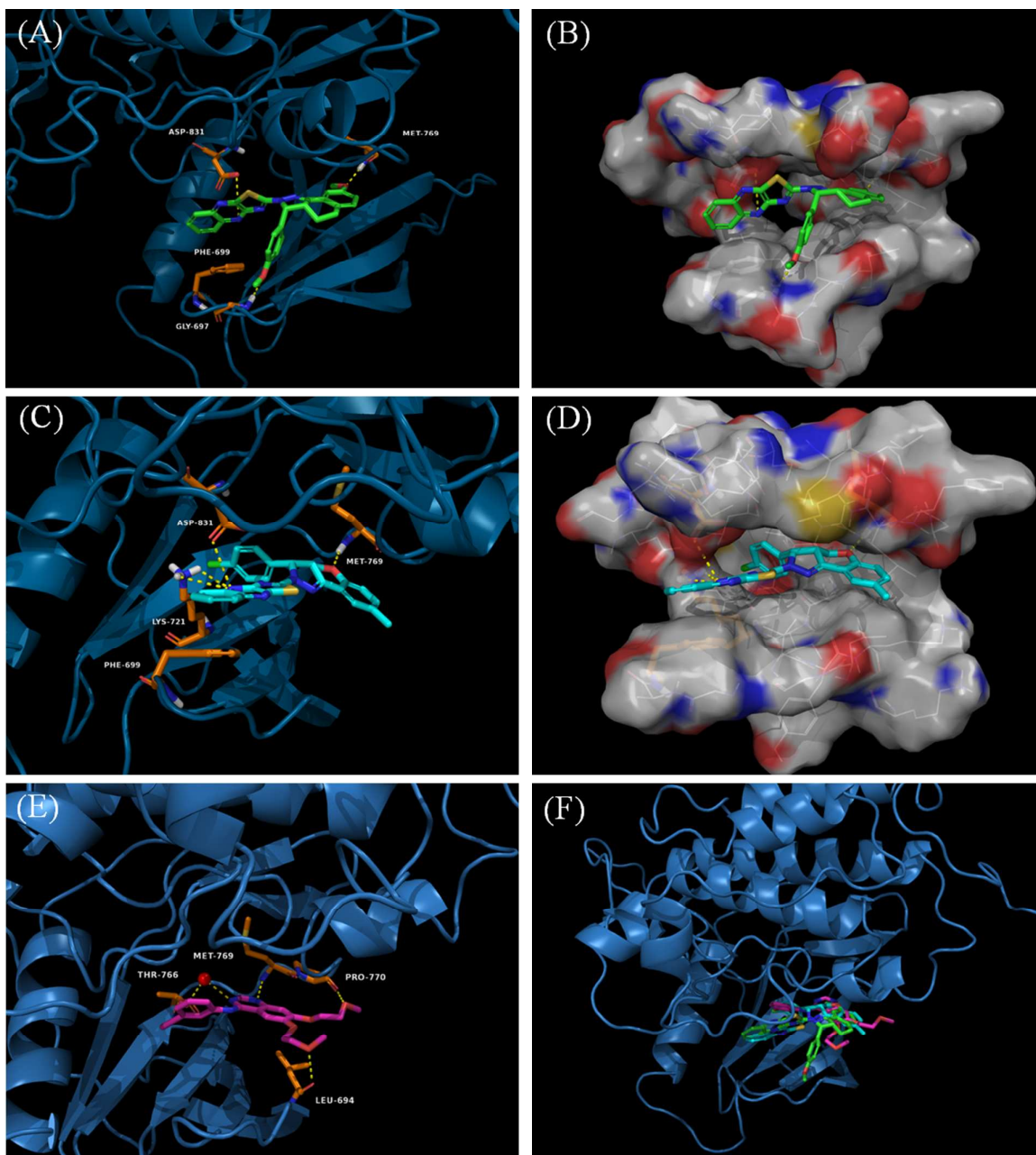
<b>4d</b>	4.80	4.64	<b>4q</b>	5.91	5.83
<b>4e</b>	5.08	5.14	<b>4r</b>	4.74	4.71
<b>4f</b>	4.97	5.12	<b>4s</b>	4.81	4.75
<b>4g</b>	5.33	5.24	<b>4t</b>	5.63	5.58
<b>4h</b>	5.74	5.61	<b>4u</b>	5.28	5.47
<b>4i</b>	5.03	5.26	<b>4v</b>	6.07	6.04
<b>4j</b>	4.82	5.00	<b>4w</b>	4.82	4.76
<b>4k</b>	5.25	5.31	<b>4x</b>	5.17	5.10
<b>4l</b>	6.55	6.54	<b>4y</b>	5.91	5.811
<b>4m</b>	5.09	4.99			



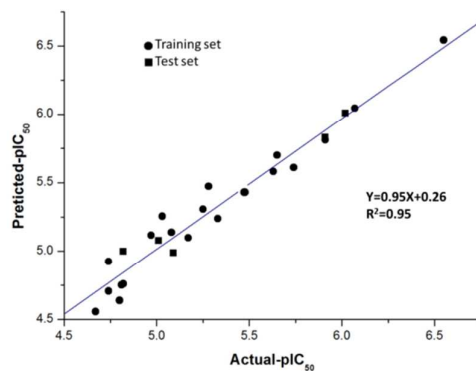
**Fig. 1** Chemical structures of EGFR and HER-2 inhibitors



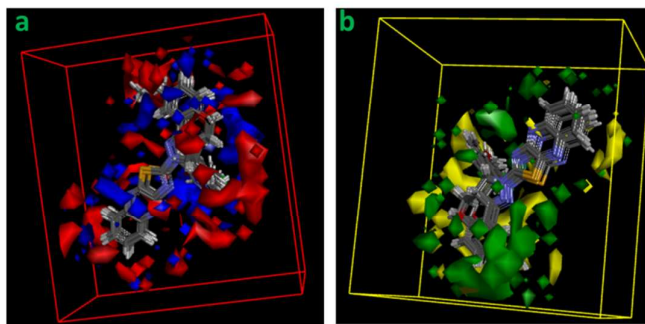
**Fig. 2** Design strategy and modification of novel EGFR/HER-2 inhibitors.



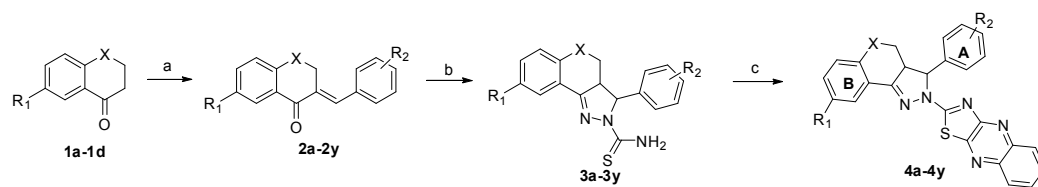
**Fig. 3** Docking modes of compounds in the binding pockets of EGFR (PDB ID: 1M17). Interactions between the protein and the ligand are shown as yellow dotted lines, the residues are shown as orange sticks, and the ligands are shown as stick models in green (**4I**), cyan (**4x**) and magenta (**Erlotinib**): (A) Predicted binding mode of **4I** with EGFR; (B) The surface of binding site of **4I** with EGFR; (C) Predicted binding mode of **4x** with EGFR; (D) The surface of binding site of **4x** with EGFR; (E) Predicted binding mode of **Erlotinib** with EGFR; (F) The docking modes of compound **4I**, **4x** and **Erlotinib** in the active site of EGFR.



**Fig. 4** Plot of experimental vs. predicted EGFR inhibitory activities of training set and test set.



**Fig. 5** (a) 3D QSAR model coefficients on electrostatic potential grids. Blue represents positive coefficients; red represents negative coefficients. (b) 3D QSAR model coefficients on van der Waals grids. Green represents positive coefficients; yellow represents negative coefficients.



**Scheme 1.** Synthetic route for the preparation of the target compounds **4a-4y**. Reagents and conditions: (a) ArCHO, 8 N NaOH, ethanol, 2 h, r.t. 65-83%; (b) thiosemicarbazide, NaOH, ethanol, 8 h, reflux, 62-75%; (c) 2,3-dichloroquinoxaline, ethanol, 8 h, reflux, 31-57%.